photochem

Article

Conformational Structure, Infrared Spectra and Light-Induced Transformations of Thymol Isolated in Noble Gas Cryomatrices

António Jorge Lopes Jesus [1,*], Cláudio M. Nunes [2] and Igor Reva [3]

[1] Faculty of Pharmacy, University of Coimbra, CQC-IMS, 3004-295 Coimbra, Portugal
[2] Department of Chemistry, University of Coimbra, CQC-IMS, 3004-535 Coimbra, Portugal; cmnunes@qui.uc.pt
[3] Department of Chemical Engineering, University of Coimbra, CIEPQPF, 3030-790 Coimbra, Portugal; reva@eq.uc.pt
* Correspondence: ajorge@ff.uc.pt

Abstract: The conformational space of the natural product thymol (2-isopropyl-5-methylphenol) was investigated using quantum chemical calculations at the B3LYP and MP2 levels, which revealed the existence of four types of conformers differing in the orientation of the isopropyl and hydroxyl groups. Thymol monomers were isolated in noble gas (Ar and Xe) matrices (at 15 K) and characterized by IR spectroscopy. With the support of B3LYP harmonic vibrational calculations, the two most stable trans-OH-conformers, differing in the isopropyl orientation, were identified in the cryomatrices. The two less stable cis-OH conformers were not detected as they shall undergo fast tunneling to the most stable ones. Annealing experiments in a Xe matrix up to 75 K did not lead to any conversion between the two isolated conformers, which is in accordance with the significative energy barrier computed for rotamerization of the bulky isopropyl group (~24 kJ mol^{-1}). Vibrational excitation promoted by broadband or by narrowband irradiation, at the 2ν(OH) frequencies of the isolated conformers, did not lead to any conversion either, which was interpreted in terms of a more efficient energy transfer to the hydroxyl rotamerization (associated with a lower energy barrier and a light H-atom) than to the isopropyl rotamerization coordinate. Broadband UV irradiation experiments (λ > 200 nm) led to a prompt transformation of matrix isolated thymol, with spectroscopic evidence suggesting the formation of isomeric alkyl-substituted cyclohexadienones, Dewar isomers and open-chain conjugated ketenes. The photochemical mechanism interpretation concords with that reported for analogous phenol derivatives.

Keywords: thymol; photochemistry; matrix-isolation; IR spectra; conformational isomerization; H-tunneling

check for updates

Citation: Lopes Jesus, A.J.; Nunes, C.M.; Reva, I. Conformational Structure, Infrared Spectra and Light-Induced Transformations of Thymol Isolated in Noble Gas Cryomatrices. *Photochem* **2022**, *2*, 405–422. https://doi.org/10.3390/photochem2020028

Academic Editors: Gulce Ogruc Ildiz and Licinia L.G. Justino

Received: 19 May 2022
Accepted: 3 June 2022
Published: 7 June 2022

Publisher's Note: MDPI stays neutral with regard to jurisdictional claims in published maps and institutional affiliations.

Copyright: © 2022 by the authors. Licensee MDPI, Basel, Switzerland. This article is an open access article distributed under the terms and conditions of the Creative Commons Attribution (CC BY) license (https://creativecommons.org/licenses/by/4.0/).

1. Introduction

Thymol (2-isopropyl-5-methylphenol, Scheme 1) is a naturally occurring monoterpenoid phenol derivative of *p*-cymene (1-isopropyl-4-methylbenzene), being one of the main chemical constituents of essential oils extracted from thyme plants. This compound is reported to exhibit, among others, antioxidant, analgesic, anti-inflammatory, antimicrobial, and anticancer activities [1–5]. Besides its pharmacological activities, thymol is also used as a flavoring and preservative ingredient in the food and cosmetic industries [6], as well as an insecticide, acaricide, and antiseptic agent [7,8].

Despite the wide range of bioactivities, the number of studies on the structure of thymol available in literature is relatively scarce [9–11]. X-ray data show that in the crystalline state, the thymol molecules are held together through O–H···O hydrogen bonds forming hexamers, which in turn are linked to each other by van der Waals contacts, while the crystal conformation is characterized by having the O–H group pointing away from the isopropyl fragment and the tertiary C–H bond of this fragment pointing towards the hydroxyl oxygen [9]. In gas phase, combination of microwave spectroscopy with theoretical calculations led to the experimental identification of three conformers for thymol, with one of them being much more populated than the other two [10].

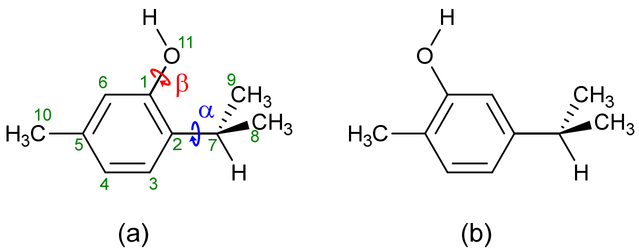

Scheme 1. Molecular structures of thymol (**a**) and carvacrol (**b**), including numbering of the heavy atoms and identification of the two conformationally relevant dihedral angles for the thymol structure. The H atoms connected to the aromatic ring are implicit.

Some infrared (IR) spectroscopic studies have been performed for thymol in the solid state [12,13] and in solution [14]. However, as far as we are aware, IR spectra of the monomeric compound have never been reported, nor has its light-induced transformations. Therefore, one of the objectives of the present paper is to fill this gap and to present, for the first time, a detailed analysis of the IR spectra of thymol isolated in low-temperature Ar and Xe matrices, and of the transformations triggered by exposing the matrix-isolated compound to IR- and UV-radiation.

Thymol is a positional isomer of carvacrol (5-isopropyl-2-methylphenol, see Scheme 1). The two molecules only differ in the relative position of the OH and isopropyl groups. In thymol, they are in *ortho*-position, while in carvacrol, they are in *meta*-position. Very recently, we have studied the conformational, vibrational and photochemical properties of carvacrol isolated in a low-temperature Ar matrix [15]. In that study, it has been shown that the molecule exists as two conformers in the cryogenic environment, differing from each other by the orientation of the isopropyl fragment. Exposition of the matrix-isolated carvacrol to broadband IR radiation was found to be effective in changing the relative population of the two conformers, by internal rotation of the bulky isopropyl fragment. A more specific goal of the current work is to verify whether this channel of vibrational energy dissipation is still effective in thymol, where the OH and isopropyl groups are closer together, making the barrier for internal rotation of the isopropyl group higher than in carvacrol.

2. Methods

2.1. Experimental Methods

Solid thymol (melting point of 49–51 °C) was supplied by Fluka with a purity degree of 99.5%. The matrix host gases (Ar N60 or Xe N48) were provided by Air Liquide. The low-temperature matrices were prepared by placing a small amount of thymol crystals into a glass tube, which was then connected to a cryostat (APD Cryogenics, Allentown, PA, USA, closed-cycle He refrigerator, with a DE-202A expander) through a needle valve, kept at ~298 K. The vapor of the sublimating compound was co-deposited with an excess of the matrix gas onto a CsI window cooled to 15 K. The temperature of the CsI window was measured directly at the sample holder by using a silicon diode temperature sensor connected to a digital controller (Scientific Instruments, Allentown, PA, USA, model 9650-1), providing the stabilization of temperature with an accuracy of 0.1 K. IR spectra of the matrix-isolated compound were recorded in the mid-IR range (4000–400 cm^{-1}) with 0.5 cm^{-1} resolution using a Nicolet 6700 Fourier-transform infrared (FTIR) spectrometer (Porto, Portugal), equipped with a deuterated triglycine sulphate (DTGS) detector (Porto, Portugal) and a KBr beam splitter (Porto, Portugal). For the experiments carried out in xenon, spectra in the near-IR (NIR) range (7500–4000 cm^{-1}, 1 cm^{-1} resolution) were also recorded using the same spectrometer equipped with an Indium Gallium Arsenide (InGaAs) detector and a CaF_2 beamsplitter.

The thymol/Xe matrix was irradiated through the outer quartz window of the cryostat by using narrowband frequency-tunable NIR light provided by the idler beam of a Quanta-

Ray MOPO-SL optical parametric oscillator (Mountain View, CA, USA) (pulse energy 10 mJ, duration 10 ns, repetition rate 10 Hz) pumped with a pulsed Nd:YAG laser. Alternatively, the sample was irradiated with broadband IR light provided by a kanthal wire electrically heated to a reddish-orange glow. Broadband UV-irradiations were also performed on the thymol/Ar matrix by using a 200 W output from a medium pressure Xe/Hg lamp (Oriel, Newport, UK).

2.2. Computational Methods

The thymol molecule has two conformational degrees of freedom, corresponding to the H–C7–C2–C1 (α) and H–O11–C1–C2 (β) dihedral angles (see Scheme 1). For identification of the conformers exhibited by this molecule, a two-dimensional (2D) potential energy surface (PES) was computed by increasing both dihedral angles in steps of 20° over the 0–360° range, in all combinations, while all the remaining internal coordinates were optimized by using the B3LYP [16–18] hybrid DFT method in conjunction with the Pople-type 6-311++G(d,p) basis set. Then, the equilibrium geometries of the thymol conformers, as well as of the putative photoproducts resulting from the UV-photolysis of the matrix-isolated compound, were fully optimized followed by harmonic vibrational calculations at the same DFT level. For the thymol conformers, calculations were also carried out by combining the second-order Møller–Plesset (MP2) perturbation method [19] with the aug-cc-pVDZ Dunning's correlation consistent basis set. Single-point energy calculations were further carried out on the MP2 optimized geometries using the QCISD method [20] combined with the same aug-cc-pVDZ basis set. The Cartesian coordinates of the B3LYP and MP2 optimized geometries of the thymol conformers are provided in Tables S1 and S2.

The B3LYP/6-311++G(d,p) harmonic wavenumbers were corrected by using the following scale factors [15,21]: 0.950 (>3200 cm^{-1}), 0.960 (3200−2000 cm^{-1}) and 0.980 (<2000 cm^{-1}). A full list of the B3LYP/6-311++G(d,p) calculated wavenumbers (scaled) and IR intensities computed for the thymol conformers are provided in Table S3. For graphical comparison with the experimental spectra, the scaled wavenumbers and IR intensities (in km mol^{-1}) were convoluted with Lorentzian functions with a full width at half-maximum (fwhm) of 2 cm^{-1} and peak heights matching the calculated IR intensities by using the Chemcraft software [22].

All quantum-mechanical computations reported in this work were performed with the Gaussian 09 software package [23], while the vibrational assignments were carried out with the vibAnalysis software [24].

3. Results and Discussion

3.1. Conformers and Barriers to Internal Interconversion

The B3LYP/6-311++G(d,p) 2D-PES calculated for thymol, as a function of the H–C7–C2–C1 (α) and H–O11–C1–C2 (β) dihedrals, is represented in Figure 1 as a contour map. Two of the four minima found on the PES exist as pairs of mirror-image structures lying within relatively broad and shallow potential energy valleys along the α coordinate, extending from −40 to +40°. One of those doubly degenerate minima is found at (α, β) = (±35°, 0°) and is designated as **gc** (**g$^+$c/g$^-$c**), while the other is located at (α, β) = (±35°, 180°) and is labeled as **gt** (**g$^+$t/g$^-$t**), where **g**$^\pm$, **c** and **t** are abbreviations of gauche plus/minus, cis and trans orientations, respectively. The first and second letters refer to the orientation around the α and β dihedrals, respectively. The **g$^+$c/g$^-$c** and **g$^+$t/g$^-$t** pairs of mirror-image structures are separated by first-order saddle points characterized by α = 0°. Two additional unique minima are found on the PES at (α, β) = (180°, 180°) and (180°, 0°) and are respectively called **tt** and **tc**. In Figure 2 are represented the geometries of the four identified thymol conformers, while in Table 1 are given their electronic (ΔE_{el}), zero-point corrected (ΔE_0) and Gibbs energies (ΔG) at 298.15 K (temperature of the gaseous compound before the matrix deposition), calculated with the B3LYP/6-311++G(d,p) and MP2/aug-cc-pVDZ model chemistries on geometries fully optimized at the respective levels. In Table 1 are included the QCISD/aug-cc-pVDZ electronic energies calculated for the MP2/aug-cc-pVDZ optimized geometries. The results of our computations are concordant with those published earlier by Schmitz et al. [10].

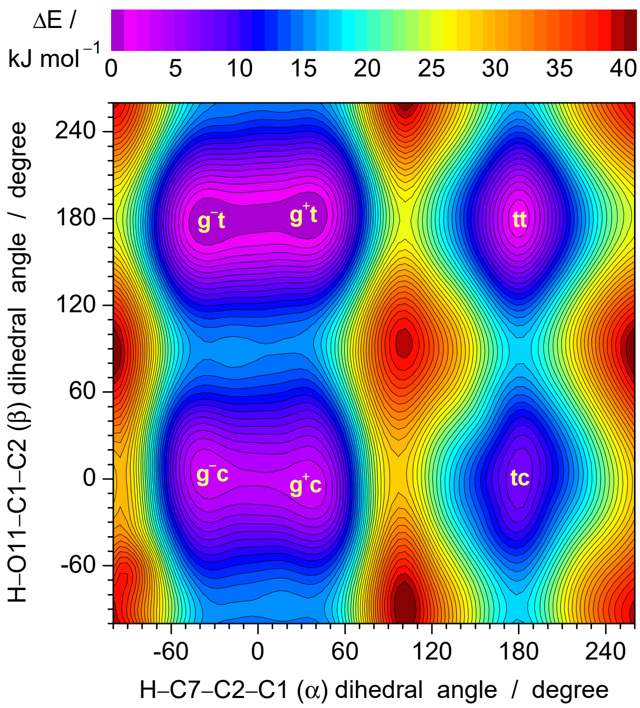

Figure 1. Contour plot of the potential energy surface computed for the thymol molecule as a function of the H−C7−C2−C1 (α) and H−O11−C1−C2 (β) dihedral angles (specified in Scheme 1). Both angles were incrementally fixed in steps of 20°, in all combinations, while all the remaining parameters were optimized at the B3LYP/6-311++G(d,p) level of theory. The minima are indicated in the plot as **gt** (**g$^+$t**/**g$^-$t**), **gc** (**g$^+$c**/**g$^-$c**), **tt** and **tc** (geometries are shown in Figure 2). The color bar on the top represents the relative energy scale (zero is assigned to the energy of the global minimum, **gt**). The isoenergy lines are traced with steps of 1 kJ mol^{-1}.

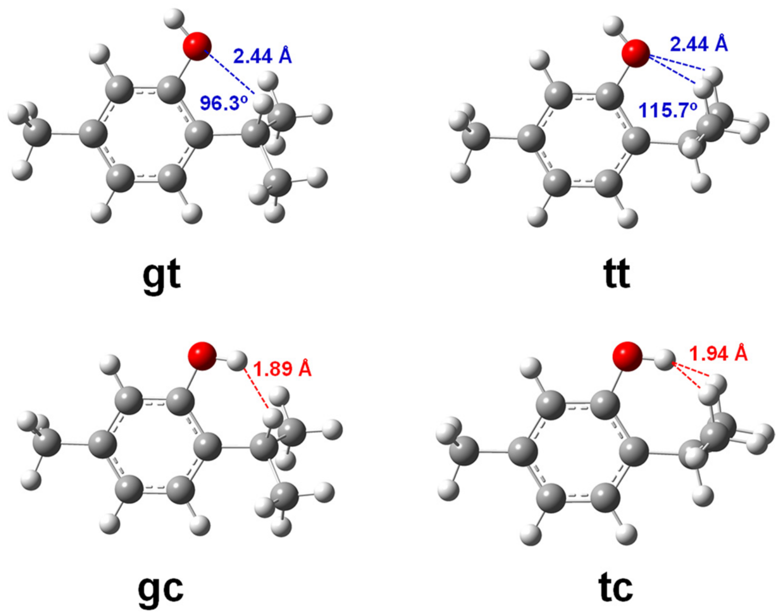

Figure 2. Geometries of the thymol conformers, including some geometrical parameters calculated at the MP2/aug-cc-pVDZ. For the doubly generated **gt** and **gc** conformers, only one of the mirror-image structures (**g$^+$t** and **g$^+$c**) is shown.

Table 1. Relative energies and Boltzmann populations calculated for the thymol conformers at different levels of theory [a].

Level of Theory	Conformer			
	gt	**tt**	**gc**	**tc**
	B3LYP/6-311++G(d,p)			
ΔE_{el}	0.00	1.37	3.24	7.34
ΔE_0	0.00	1.11	3.54	6.07
ΔG (298 K)	0.00	1.27	4.96	5.18
Pop. (%)	66.9	20.0	9.0	4.1
	(75.9)	(24.1)		
	MP2/aug-cc-pVDZ			
ΔE_{el}	0.00	2.51	2.54	7.94
ΔE_0	0.00	1.94	2.43	7.01
ΔG (298 K)	0.00	1.52	2.12	5.43
Pop. (%)	57.0	15.5	24.3	3.2
	(81.3)	(18.7)		
	QCISD/aug-cc-pVDZ [b]			
ΔE_{el}	0.00	2.29	2.56	7.30

[a] ΔE_{el}—relative electronic energy; ΔE_0—relative electronic energy corrected for zero-point vibrational energy; ΔG—relative Gibbs energy at 298 K; all relative energies are expressed in kJ mol^{-1} and were calculated with respect to the energy of the most stable conformer **gt**. Equilibrium populations (Pop.) were estimated by means of the Boltzmann distribution based on the ΔG values at 298 K (weighting factors of 2/2 or 1/1 were used for conformers **gt**/**gc** or **tt**/**tc**, respectively). Values in parentheses correspond to the expected populations of conformers **gt** and **tt** with the contributions of the populations of conformers **gc** and **tc**, respectively. [b] Single-point calculations performed on the MP2/aug-cc-pVDZ optimized geometries.

At all levels of theory, **gt** is the lowest-energy conformer. It has the hydroxyl group pointing away from of the isopropyl fragment, while the C7–H bond is ± gauche with respect to the C2–C1 bond (see Figure 2), with α taking values of ±35.6° (B3LYP) or ±39.0° (MP2). The deviation of the C7–H bond from the aromatic ring plane should be attributed to the presence of the hydroxyl group in *ortho*-position relative to the isopropyl fragment, a feature also observed in a structural microwave spectroscopic study of the 2,6-diisopropylphenol analog [25]. Note that in carvacrol or *p*-isopropylphenol, where the OH and isopropyl substituents occupy *meta*- or *para*-positions, respectively, all conformers identified for these molecules were found to have the tertiary C–H bond of the isopropyl group lying in the aromatic ring plane [15,26,27]. The geometry of **gt** is not too different from that adopted by the thymol molecules in the crystal, although in the latter case the C7–H bond is less deviated from the ring plane (α = ±13.3°) [9]. The second most stable conformer, **tt**, also has the hydroxyl group pointing away from the isopropyl fragment, but the C7–H and C2–C1 bonds are trans to each other, bringing the two methyl groups of the isopropyl close to the oxygen atom (Figure 2). This conformational arrangement results in an increase of the electronic, zero-point corrected, or Gibbs energies by 1.1–2.5 kJ mol^{-1} relative to the global minimum.

As shown in Figure 2, the (C7)H···O distance in **gt** and the (C8)H···O (equivalent of (C9)H···O) distance in **tt** are smaller than the sum of the van der Waals radii of the oxygen and hydrogen atoms (2.72 Å). This suggests the formation of C–H···O interactions in both trans-OH-conformers, as has been claimed in previous studies carried out for thymol [10] and 2-isopropylphenol [28]. These interactions, however, should be very weak because of the significant deviation of the C–H···O bonding angles (96–116°) from the linearity: it is well known that the strongest nonbonded interactions are observed for the linear arrangements (optimal value of 180°) [29,30]. In the **gc** and **tc** conformers, the hydroxyl group is directed towards the isopropyl fragment. Such an orientation does not allow the formation of stabilizing C–H···O interactions. Instead, it originates one (**gc**) or two (**tc**) repulsive CH···HO close contacts (see Figure 2). Both factors explain the lower stability of these cis-OH-conformers, and in particular of **tc**, relative to the **gt** and **tt** ones.

To characterize the conformational composition of the gaseous sample of thymol immediately before the matrix deposition, the populations of the thymol conformers in the gaseous phase were estimated from the values of ΔG at 298.15 K, through the application of the Boltzmann statistics, and the obtained values have been included in Table 1. According to these estimates, **gt** is by far the most abundant conformer in the gaseous phase, with a population of 57–67%. Conformer **tt** is also predicted to be present in the gaseous phase, but in a smaller amount (15–20%), while the population of conformer **gc** is of only 9% when it is estimated from the B3LYP Gibbs energies, increasing to 24% when obtained from the MP2 Gibbs energies. Nevertheless, as will be shown below, the difference of population predicted for this conformer by the two theoretical methods is not relevant from the experimental viewpoint. Finally, a very small the gaseous phase abundance (3–4%) is predicted for the less-stable **tc** conformer.

For the interpretation of the results of the matrix-isolation experiments, it is also relevant to have an idea of the energy barriers corresponding to the conversion of the higher into the lower energy conformers [31–33]. In Figure 3 are represented the OH-torsional barriers interconnecting the pair of conformers (**gc** and **gt**), and the pair of conformers (**tc** and **tt**). The heights of these barriers in the direction of conformational relaxation were calculated to be 10–12 kJ mol^{-1}. These values are of the same order as those computed for the conversion of higher into lower energy OH-rotamers in various compounds containing the phenol moiety, such as 2-cyanophenol (15 kJ mol^{-1}) [34], 2-isocyanophenol (12 kJ mol^{-1}) [35], hydroquinone (11 kJ mol^{-1}) [36], tetrachlorohydroquinone (19 kJ mol^{-1}) [37], and carvacrol (16 kJ mol^{-1}) [21]. Although these energy barriers are too high to be surmounted in a low-temperature matrix environment, for all these previously studied derivatives of phenol compounds, the higher energy OH-rotamers escaped from spectroscopic detection in matrixes of inert gases because of their fast depopulation in favor of the corresponding lower energy OH-rotamers by means of quantum tunneling of hydrogen atom [38,39]. The same behavior has been reported in various matrix-isolation studies carried out for other compounds containing conformers differing from each other by 180° rotation of an OH group, namely carboxylic acids [40–44] and aminoacids [45]. Therefore, it is expected that in the case of thymol, the **gc** and **tc** cis-OH-conformers shall also undergo fast tunneling OH rotamerization to the respective **gt** and **tt** trans-OH-forms in the low temperature Ar and Xe matrices, thus preventing experimental identification of the cis-OH-forms.

To theoretically address this issue, we carried out computations of reaction paths for the flip of the OH group in the (**gc**, **gt**) and (**tc**, **tt**) pairs of conformers. Initially, the first-order transition states for OH-torsion were optimized, and the respective force constants were computed analytically. The intrinsic reaction paths were then followed from the transition states in both directions. The intrinsic reaction coordinate (IRC) was set using the "IRC = Cartesian" option of the Gaussian software and is expressed in units of Bohr. The computed reaction paths for the OH torsion in the (**gc**, **gt**) and (**tc**, **tt**) pairs are presented in Figure 3.

The probability of tunneling through a parabolic barrier was estimated by using the equation

$$P(E) = e^{-4\pi w\sqrt{2mE}/h} \tag{1}$$

where a particle with mass m tunnels through a barrier with height E and width w, and h is the Planck constant [38,39]. Using the calculated barrier heights E of 10.32 and 8.57 kJ mol^{-1} and widths w of 2.915 and 2.715 Bohr for the **gc** → **gt** and **tc** → **tt** conversions, respectively, one can estimate the tunneling probability (transmission coefficient) of the light H-atom (m = 1) in **gc** as 2.97 × 10^{-8}, and in **tc** as 4.08 × 10^{-7}. The tunneling rate is a product of the transmission coefficient and the frequency of attempts. Assuming that the OH group is vibrating at an OH torsional frequency of 317 cm^{-1} in **gc** and 275 cm^{-1} in **tc** (computed values), tunneling rates of 2.82 × 10^{5} s^{-1} (half-life time of ~2.5 microseconds) and 3.36 × 10^{6} s^{-1} (half-life time of ~0.2 microseconds) were estimated for the **gc** → **gt** and **tc** → **tt** rotamerizations, respectively. According to these results, there is no doubt that the

gc and **tc** conformers are unlikely to survive long enough in low temperature Ar and Xe matrices to allow their spectroscopic detection.

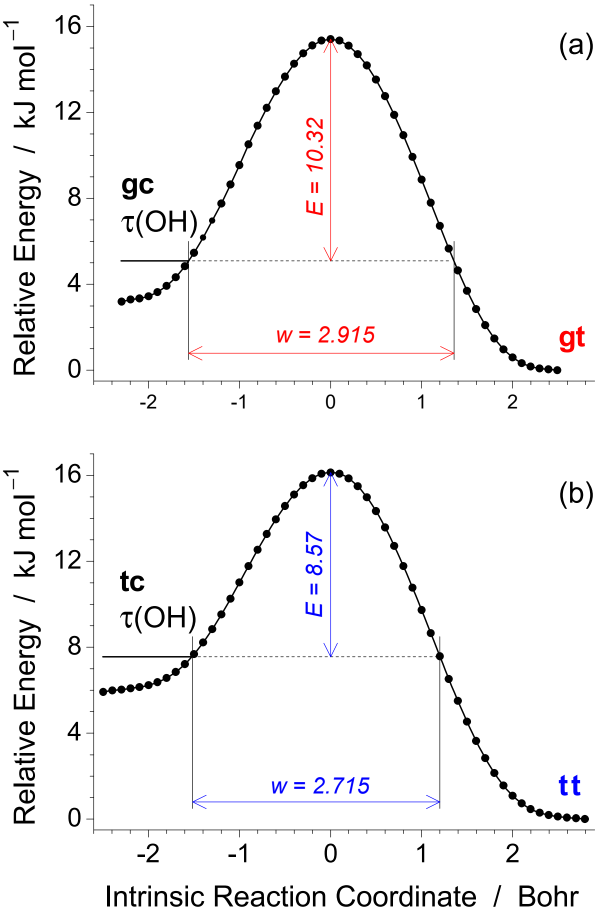

Figure 3. IRC profiles for the flip of OH-group in (**gc**, **gt**) (**a**) and (**tc**, **tt**) (**b**) pairs of thymol conformers, computed at the B3LYP/6-311++G(d,p) level of theory in Cartesian (non-mass-weighted) coordinates. The vertical arrows (E = 10.32 or 8.57 kJ mol^{-1}) designate the computed ZPE-corrected energies of the transition states with respect to the reactants (**gc** or **tc**, left in each frame). The horizontal arrows designate the estimated barrier widths (w = 2.915 or 2.715 Bohr) of the barrier at the ZPE level of the reactants. The relative zero energies correspond to the products (**gt** or **tt**, right in each frame).

Conversion of the **tt** into the **gt** conformer involves the internal rotation of a bulky isopropyl group and should only occur through an over-the-barrier mechanism. The torsional barrier for this isomerization was computed to be ~24 kJ mol^{-1} (see Figures 1 and S1). This value is too high to allow the occurrence of a **tt** → **gt** relaxation in a matrix environment at a temperature as low as 15 K [46,47]. Accordingly, both conformers are expected to be trapped in the as-deposited Ar and Xe matrixes with populations of 76–81% (**gt**) and 24–19% (**tt**). These values were obtained by considering the conversion of the estimated gas phase populations of **gc** to **gt** and of **tc** to **tt** (see Table 1).

It is interesting to compare the potential energy profile for the rotation of the isopropyl group in thymol with that computed for the closely related carvacrol and *p*-cymene molecules (see Figure S1). The heights of the barriers separating the conformers of these last two molecules differing from each other by internal rotation of the isopropyl group are ~10 kJ mol^{-1}, which is 2.5 times lower than the one computed for thymol. For these three molecules, the first-order transition state separating the conformers is characterized by having the tertiary C-H bond of the isopropyl group nearly perpendicular to the aromatic ring plane. In *p*-cymene and carvacrol, this gives rise to steric repulsions between the two methyl groups of the isopropyl fragment and their neighboring aromatic C-H bonds, whereas in thymol, one of the methyl groups stays too close to the OH group, leading to stronger steric repulsions, which is responsible for the significant increase in the barrier height associated with the isopropyl group rotamerization. As it will be shown below, this result has important implications for the outcomes of the experiments of thermal and IR excitations carried out for matrix-isolated thymol.

3.2. Infrared Spectra of Matrix-Isolated Thymol, Annealing and IR Irradiations

Monomers of thymol were trapped in Ar and Xe matrixes at 15 K, as described in Section 2.2, and the mid-IR spectra recorded for the freshly deposited samples are shown in Figure 4a,b (3675–3580 and 1650–700 cm^{-1} regions), while the spectral positions and relative intensities (expressed qualitatively) of the observed bands are collected in Table 2. The two experimental spectra are well reproduced by the population-weighted theoretical spectrum of the matrix-isolated compound, which is displayed in Figure 4c. This spectrum was obtained by summing the individual spectra calculated for the conformers present in the matrix, shown in Figure 4d, with the computed IR intensities weighted by their expected populations in the noble gas matrices: 0.79 for **gt** and 0.21 for **tt** (mean values obtained from the B3LYP and MP2 computations, see Table 1). From the comparison of the experimental and theoretical spectra, an assignment of the experimental bands was carried out and has been included in Table 2.

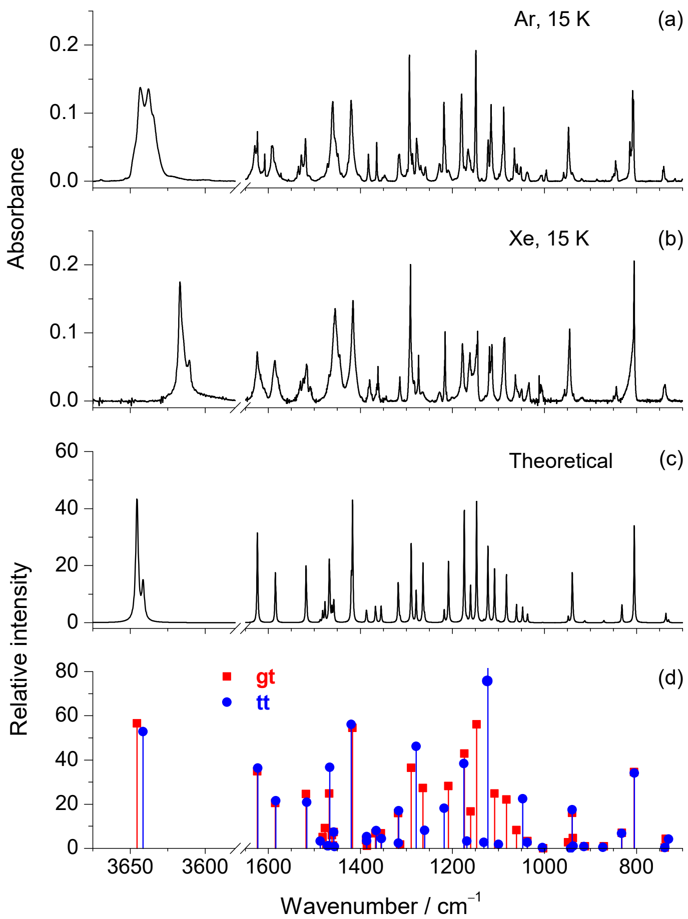

Figure 4. Experimental IR spectra of thymol isolated in (**a**) Ar and (**b**) Xe matrices at 15 K; (**c**) Theoretical IR spectrum of thymol, obtained as a sum of the B3LYP/6-311++G(d,p) spectra calculated for the two experimentally relevant conformers with their intensities scaled by the respective expected populations in the noble gas matrices. This spectrum was simulated by applying Lorentzian functions (fwhm = 2 cm^{-1}) centered at the scaled wavenumbers; (**d**) Scaled wavenumbers and unscaled IR intensities extracted from the harmonic vibrational calculations carried out at the B3LYP/6-311++G(d,p) level for the **gt** and **tt** conformers.

Table 2. Bands observed in the experimental IR spectra of thymol isolated in Ar and Xe matrices, compared with the harmonic wavenumbers ($\tilde{\upsilon}$/cm^{-1}) and absolute IR intensities (Ath/km mol^{-1}) calculated for the **gt** and **tt** conformers at the B3LYP/6-311++G(d,p) level, and vibrational assignment.

Ar, 15 K [a]		Xe, 15 K [a]		Calc. gt [b]		Calc. tt [b]		Assignment [c]
$\tilde{\upsilon}$	Int.	$\tilde{\upsilon}$	Int.	$\tilde{\upsilon}$	Ath	$\tilde{\upsilon}$	Ath	
3643/3638/ 3635 (sh)	vs	**3617**/3611	vs	3645.5	56.6	3641.5	52.8	ν(OH)
1629	m	1624	m	1623.9	34.9	1622.9	36.3	ν(CC)$_{ring}$
1591	m	1586	m	1584.8	20.6	1583.5	21.5	ν(CC)$_{ring}$
1519 (split)	m	1517 (split)	m	1518.2	24.7	1516.5	20.5	ν(CC)$_{ring}$; δ(CH)$_{ring}$
				1481.9	5.1	1487.3	3.3	δ(CH_3)$_{iso,as'}$ (+)
				1476.9	9.2	1471.4	1.1	δ(CH_3)$_{iso,as''}$ (+)
1460 (split)	s	1455 (split)	s	1467.7	24.8	1466.3	36.7	δ(CH_3)$_{as'}$
				1461.7	6.0	1456.6	0.8	δ(CH_3)$_{iso,as''}$ (−)
				1459.3	1.3	1469.3	1.4	δ(CH_3)$_{iso,as'}$ (−)
				1457.6	7.3	1458.0	7.3	δ(CH_3)$_{as''}$
1420	s	1416	s	1417.0	54.5	1420.0	56.6	δ(CH)$_{ring}$; ν(CC)$_{ring}$; ν(CO)
1383	w	1380	w	1387.4	3.8	1386.3	3.4	δ(CH_3)$_{iso,s}$ (+)
				1385.5	1.1	1386.5	5.3	δ(CH_3)$_s$
1365	w	1362	w	1367.4	6.8	1365.8	8.0	δ(CH_3)$_{iso,s}$ (−)
1347	vw	1344	vw	1355.1	6.8	1355.1	4.6	δ(C7H)
1315	w	1314	w	1318.0	16.0	1316.6	17.1	ν(CC)$_{ring}$; δ(OH)
				1313.7	1.7	1317.6	2.3	γ(C7H)
1294/1287	vs	**1291**/1284	vs	1289.8	36.5	–	–	ν(CC)$_{ring}$; δ(CH)$_{ring}$
1278	m	1274	m	–	–	1278.9	46.2	ν(CC)$_{ring}$; δ(CH)$_{ring}$
1269/1259	vw	1265	vw	1264.0	27.4	1260.5	8.1	ν(CO) + ν(C5C10); ν(CC)$_{ring}$
1228	vw	1228	vw	–	–	1218.4	18.2	ν(C2C7)
1219	s	1216	s	1208.7	28.2	–	–	ν(C2C7)
1180	s	1179	m	1174.4	42.8	1175.0	38.3	δ(OH); δ(C–H)$_{ring}$
				–	–	1168.7	3.2	ν(CO) − ν(C5C10); δ(CH)$_{ring}$
1166	w	1162	m	1160.8	16.7	–	–	ν(CO) − ν(C5C10); δ(CH)$_{ring}$
1149	vs	1147/**1145**	s	1147.7	56.1	–	–	δ(OH); δ(CH)$_{ring}$; ν(CC)$_{ring}$
1123	m	1120	m	–	–	1123.1	111.8	δ(ring); δ(OH); ν(CO)
1116	m	1115	m	1108.7	24.8	–	–	ν(C7C8) − ν(C7C9)
1089	m	1087	m	1082.6	22.1	–	–	δ(ring)
1065/1059	w	1063	w	1060.7	8.3	–	–	ρ(CH_3)$_{iso}$ (+)
1051	vw	1049	vw	–	–	1047.4	22.5	ρ(CH_3)$_{iso}$ (+)
1037	vw	1034	vw	1036.7	3.2	1037.2	2.7	ρ(CH_3)′
1007/996	vw	1008	vw	–	–	–	–	–
959	vw	956	vw	948.3	2.7	–	–	ρ(CH_3)$_{iso}$ (−)
948/940	m	**945**/937	m	939.6	16.0	939.7	17.5	ν(CO) − ν(C5C10); δ(ring)
918	vw	918	vw	912.4	0.9	914.2	0.8	ρ(CH_3)$_{iso}$ (−); γ(C7H)
886	vw	n.o.		870.8	1.0	872.8	0.5	ν(C7C8) + ν(C7C9)
849/**846**	vw	850/**844**	vw	831.6	7.0	832.4	6.8	γ(C6H)
814/**809**/807	s	805	vs	805.0	34.5	805.1	33.8	γ(C3H) + γ(C4H)
741	vw	738	vw	736.3	4.3	730.5	4.1	δ(ring)
700	vw	n.o.		681.3	1.3	684.0	4.9	ν(C2C7) − ν(C5C10); δ(ring)
594	w	593	w	594.0	7.8	594.6	8.5	γ(C5)
577	w	577	w	571.5	12.9	576.9	6.4	δ(ring)

[a] Absorptions falling in the 3100–2800 cm^{-1} range, corresponding to the CH and CH_3 stretching vibrations, were not analyzed. Experimental intensities (Int.) are expressed qualitatively: vs = very strong; s = strong; m = medium; w = weak; vw = very weak. The most intense component of each multiplet band is highlighted in bold. [b] Calculated harmonic wavenumbers are scaled by 0.980 and 0.950, for the regions below 2000 cm^{-1} and above 3200 cm^{-1}, respectively. Some weak calculated absorptions with no correspondence in the experimental spectrum are not included (a full list of the vibrations calculated for the two conformers is provided in Table S3). [c] Based on the results provided by the "vibAnalysis" software [24] supported by ChemCraft animation of the vibrations. Atom numbering is presented in Scheme 1. Abbreviations: ν, stretching; δ, in-plane deformation; γ, out-of-plane deformation; τ, torsion; ρ, rocking; as, antisymmetric; s, symmetric; iso, isopropyl group, sh, shoulder. Signs "+" and "−" designate combinations of vibrations in the same phase and in the opposite phase, respectively.

The intense band observed in the experimental spectra at wavenumbers above 3600 cm^{-1} is assigned to the stretching vibration of the OH group (νOH). In the spectrum of thymol recorded in Ar matrix, this band appears as a relatively broad and split feature with two main components at 3643 and 3638 cm^{-1} and a shoulder at ~3635 cm^{-1}. OH stretching bands at practically the same positions have been identified in the IR spectra of phenol [48] (also having two main components) and of some phenol derivatives such as tyramine [49] and carvacrol [15], isolated in solid Ar. In the spectrum of thymol trapped in Xe, the νOH band is sharper and appears as a doublet at 3617/3611 cm^{-1}, shifted to lower frequencies, as compared with thymol in Ar. Such a shift of the OH-stretching frequency is typical for matrix-isolated compounds [32,33]. In this range, the spectrum of thymol in a xenon matrix exhibits a very similar profile to that of the population-weighted theoretical spectrum. This similarity suggests that the higher and lower frequency band components in the experimental spectrum are assigned, respectively, to the **gt** and **tt** conformers, which agrees with the order of wavenumbers predicted for the νOH absorptions of the two rotamers: 3645.5 cm^{-1} (A^{th} = 56.6 km mol^{-1}) for **gt** and 3641.5 cm^{-1} (A^{th} = 52.8 km mol^{-1}) for **tt**.

In the fingerprint region, a detailed comparison of the experimental and theoretical spectra allows the identification of seven bands that can be assigned to the most populated **gt** conformer. These bands appear between 1300 and 1000 cm^{-1} and are centered in the spectra recorded in Ar/Xe at 1294/1291, 1219/1216, 1166/1162, 1149/1145, 1116/1115, 1089/1087 and 1065/1063 cm^{-1}, while the corresponding theoretical absorptions are predicted at 1289.8, 1208.7, 1160.8, 1147.7, 1108.7, 1082.6 and 1060.7 cm^{-1}. Spectral markers of the **tt** conformer are located at 1278/1274, 1228/1228, 1123/1120 and 1051/1049 cm^{-1} (see Table 2), with the respective calculated absorptions predicted at 1278.9, 1218.4, 1123.1 and 1047.4 cm^{-1}.

As we have mentioned in the previous section, the **gc** and **tc** conformers are not expected to be present in the as-deposited matrixes because of their fast depopulation (on the microsecond time scale) in favor of the **gt** and **tt** forms by quantum mechanical tunneling during deposition of the matrixes. This is experimentally supported by a thorough comparison between the experimental and calculated spectra shown in Figure S2, where intense absorptions calculated for the two higher-energy forms have no correspondence in the experimental spectra.

The experimental populations of the two matrix-populated conformers were estimated from the integrated intensities of selected pairs of band components (Ar: 1294/1278, 1219/1228, 1149/1123; Xe: 3617/3611, 1291/1274, 1216/1228, 1145/1120), normalized by the calculated absolute intensities of the corresponding vibration modes. The obtained values were 75 ± 6% for **gt** and 25 ± 6% for **tt**, which are in good concordance with the theoretical predictions. This gives an approximate **gt**:**tt** experimental ratio of 3:1, which will be discussed later on in this paper.

One attempt to promote conversion between the two rotamers in the matrix, in order to allow their unequivocal identification, consisted of performing annealing experiments. Taking into consideration the magnitude of the energy barrier corresponding to the conversion of the **tt** into the **gt** conformer (~24 kJ mol^{-1}), this conformational relaxation may only be observed in a matrix with stronger relaxant properties and with the possibility of heating to the highest possible temperature. Xe matrix was therefore the obvious choice for performing these experiments. The sample was annealed up to 75 K, which is the upper limit of thermal stability of solid xenon. However, no changes in the band intensities were observed that could be attributed to the conversion of the higher energy conformer into the most stable form. Apparently, the high energy barrier separating the two matrix-isolated conformers, combined with necessity of internal torsion of a bulky isopropyl group, precludes the occurrence of a **tt** → **gt** relaxation in the Xe matrix, even upon heating the sample at a temperature as high as 75 K. According to the correlation proposed by Barnes [50], a temperature above 80 K would be needed to overcome an energy barrier of ~24 kJ mol^{-1}. Hence, the non-observation of a thermally induced **tt** → **gt** relaxation is not surprising under the present experimental conditions.

Another attempt to induce changes in the population of the two matrix populated conformers consisted of the excitation of monomers of thymol isolated in solid Xe with narrowband or broadband IR radiation. The narrowband IR excitations were undertaken by tuning the optical parametric oscillator at the first overtone of the OH stretching vibration (2νOH). Before performing the irradiations, a near-IR spectrum was recorded to identify the position of the 2νOH band. This band appears as a doublet with a main component centered at 7061 cm^{-1}, and a shoulder at 7047 cm^{-1} (see Figure S3), which is very close to its position observed in the near-IR spectrum of thymol dissolved in CCl_4 solution (7056 cm^{-1}) [14]. The shape of the 2νOH band is identical to that of the fundamental νOH feature observed in the mid-IR spectrum, meaning that the higher and lower frequency components should be ascribed, respectively, to the 2νOH absorptions of the **gt** and **tt** conformers. Absorption of a near-IR photon with wavenumber in the 7061−7047 cm^{-1} range introduces in the molecule an energy of ~84 kJ mol^{-1}. This amount of excitation energy is 3.5 times larger than the barrier height computed for the interconversion between the conformers in both directions, which, in principle, is more than sufficient to overcome the barrier for conformational isomerization for a free monomer in the gas phase by internal rotation of the isopropyl group. However, exposure of thymol isolated in a Xe matrix to laser light tuned to 7061 or 7047 cm^{-1} for ~30 min did not result in any spectral modifications that could indicate that a conformational transformation had occurred. We also attempted to promote changes in the population of the two matrix-isolated conformers by letting the matrix be exposed to broadband IR-radiation emitted from a kanthal wire electrically heated to a reddish-orange glow, a methodology that has been successfully applied by us to induce changes in the relative abundances of the two conformers of the structurally similar carvacrol isolated in an Ar matrix [15]. However, in the present case, we did not observe any spectral indications of the occurrence of conformational changes.

A possible explanation for the lack of infrared-induced conformational isomerization of the isopropyl group in thymol **tt** or **gt** is that the energy deposited in the 2νOH mode is more efficiently transferred to the lower energy OH-rotamerization coordinate (Figure 5), which will result in the isomerization of **tt** into **tc** or **gt** into **gc**. However, because **tc** and **gc** are high-energy cis-OH conformers that should decay very fast by H-tunneling back to the most stable **tt** and **gt** trans-OH-forms, respectively, no spectral changes would be observed in the course of the infrared irradiation experiments monitored using steady-state spectroscopy. Interestingly, as shown in Figure 5, in comparison with thymol, the carvacrol molecule has the C_3H_7 and OH competitive rotamerizations with an opposite barrier height trend. That feature is likely to provide for carvacrol a more efficient energy transfer to its lower energy C_3H_7 rotamerization coordinate, even when the energy is deposited in the 2ν(OH) or ν(OH) mode. This explains why the conformational isomerization of the isopropyl group in carvacrol was previously observed upon broadband IR irradiation [15].

3.3. UV-Induced Transformations

Monomers of thymol **1** isolated in a low temperature Ar matrix were subjected to irradiation with broadband UV-light at $\lambda > 200$ nm emitted directly from a Xe/Hg lamp. The experimental conditions for the UV-irradiations were established taking into consideration the UV-spectrum of thymol in methanol solution, which exhibits absorption maxima at λ = 221 and 280 nm [13]. The times of exposition of the sample to the UV-light varied from 2 to 120 min. After each irradiation, an IR spectrum was collected to monitor the transformations occurring in the matrix-isolated compound.

Spectral indication of occurrence of photoreactions started to be observed shortly after the first four minutes of irradiation. The most notorious spectral change was the appearance of a relatively broad feature within the 2125–2090 cm^{-1} range, centered at ~2106 cm^{-1} (see Figure 6a). This band is very characteristic of the antisymmetric stretching vibration of the ketene group [ν_{as}(C=C=O)] [21,48,51–54], thus revealing the photogeneration of compounds bearing this fragment. According to the results of previous photochemical studies carried out for matrix-isolated compounds containing the phenol [15,21,48,49,54,55] moiety, the photoreaction pathway leading to the formation of ketenes is initiated by detachment of the H-atom from the O–H bond in **1**. Then, recombination of the released H-atom with the highly reactive phenoxyl-type radical **2** at the *ortho*- or *para*- ring carbon atoms with respect to the CO group, gives rise to alkyl-substituted cyclohexadienones, which may exist in three isomeric forms, labeled as **3a**, **3b** and **3c** (see Scheme 2). The preference of the H-atom to reconnect at these ring positions is theoretically supported by the results of an NBO analysis carried out at the B3LYP/6-311++G(d,p) level for **2**. In fact, besides the oxygen atom, atoms C2, C4 and C6 are those exhibiting, by far, the largest natural spin densities (see Figure S4). The presence of **3** in the UV-irradiated thymol/Ar matrix is spectroscopically confirmed by the appearance of two bands at 1677 and 1659 cm^{-1} (Figure 6a), which are typical positions of the stretching vibration of a C=O group in cyclohexadienones [15,21,48,56]. Finally, cleavage of the weaker C–C bond at α-position with respect to the C=O group in **3a** or **3b**, yields open-chain conjugated ketenes **5a** or **5b**, respectively (Scheme 2).

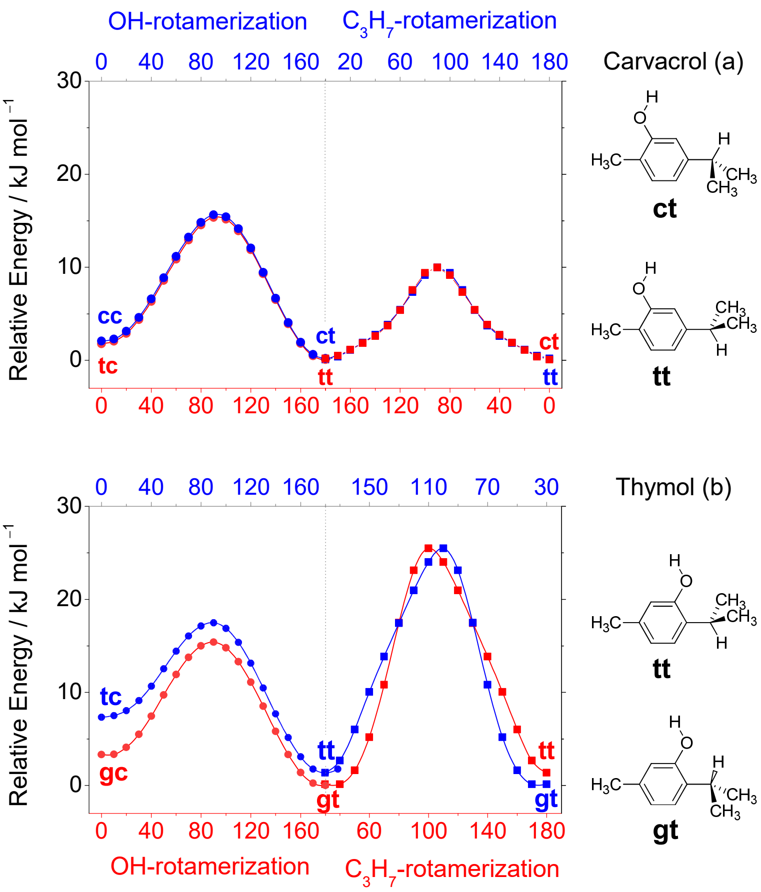

Figure 5. B3LYP/6-311++G(d,p) relaxed potential energy scans calculated for (**a**) carvacrol and (**b**) thymol regarding the rotamerization of the hydroxy (OH) and isopropyl (C_3H_7) groups. The bottom and top x-axis (red and blue) refer to the corresponding dihedral angle changes of the first and second most stable conformations, respectively, which are illustrated for each species at the right side of the panel. The conformers of carvacrol are designated according to the scheme adopted in this work for thymol: the first letter designates the orientation of the tertiary C–H bond of the isopropyl fragment relative to the C–O bond, while the second refers to the orientation of the O–H group relative to the vicinal alkyl group.

To theoretically support the proposed assignments, we have carried out full geometry optimizations and harmonic vibrational calculations for the relevant isomeric forms adopted by **3** and **5**, which are characterized in Tables S4–S6. For species **5**, only the structures adopting *Z*-configuration around the central C=C bond have been considered in the calculations. This assumption was based on the results of a recent study on the photochemistry of 1,3-cyclohexadiene isolated in solid parahydrogen, where only the *Z*-type isomers of the open-ring photoproducts were found to appear during the initial stages of the UV-irradiations [57]. The range of wavenumbers predicted for the ν_{as}(C=C=O) mode of **5** was 2106–2084 cm^{-1} (A^{th} = 637–1485 km mol^{-1}) and for the ν(C=O) mode of **3** was

1679–1654 cm^{-1} (A^{th} = 165–318 km mol^{-1}). These values are very close to the positions of the new observed absorptions of photoproducts, emerging upon UV-irradiations of thymol (Figure 6). We also tried to identify a spectral signature of **2**. However, the few strong infrared absorptions predicted for this species could not be observed experimentally, which is not surprising, due to its high reactivity.

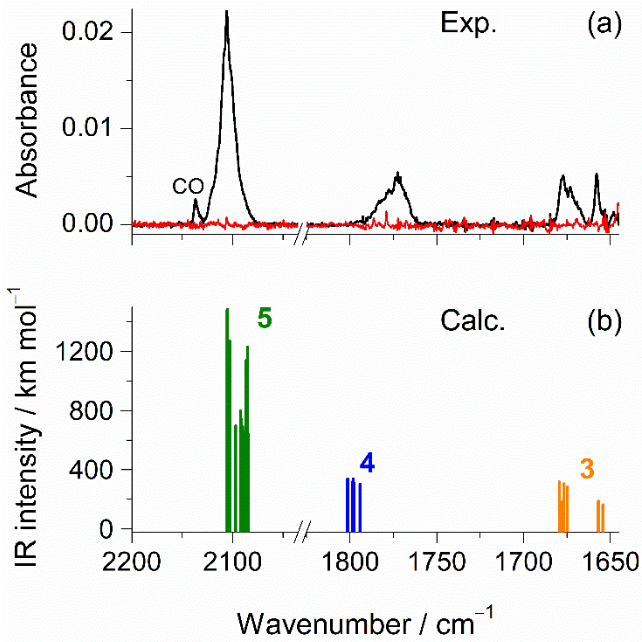

Figure 6. (**a**) Fragment of the IR spectrum of thymol **1** (Ar, 15 K) recorded after 4 min of UV-irradiation (black trace) and before any UV-irradiation (red trace). (**b**) B3LYP/6-311++G(d,p) calculated wavenumbers (scaled) and IR intensities corresponding to the antisymmetric C=C=O stretching modes of all surveyed isomeric forms of the open-ring ketenes **5** (green), C=O stretching modes of all Dewar valence isomers **4** (blue), and C=O stretching modes of all isomeric forms of the alkyl-substituted cyclohexadienones **3** (orange). For the structures of **3**, **4**, **5**, see Scheme 2.

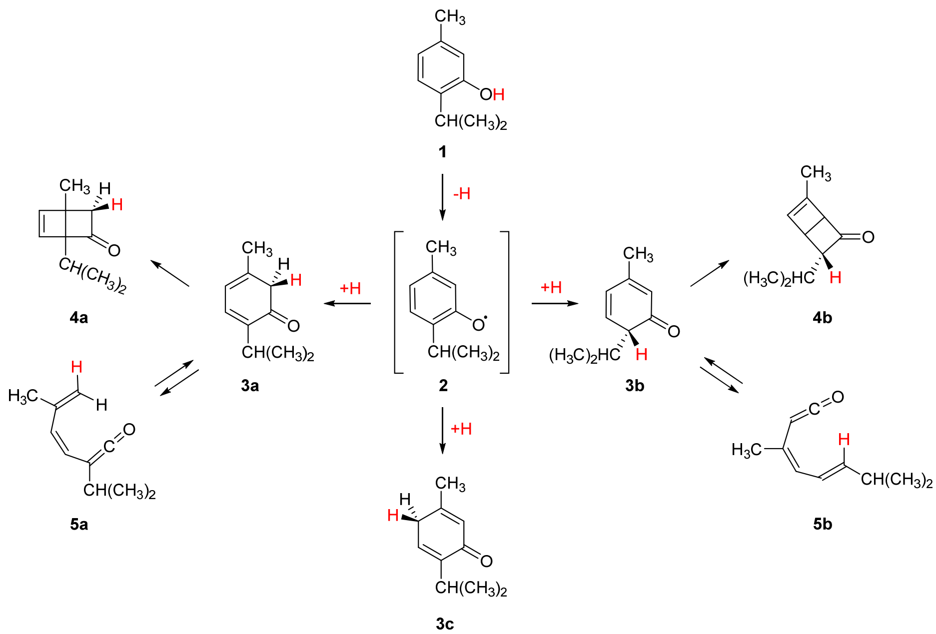

Scheme 2. UV-induced isomerizations experimentally observed for thymol **1** isolated in solid Ar at 15 K.

Alongside with the IR bands assigned to **3** and **5**, a new band centered at ~1773 cm^{-1} was also observed in the infrared spectra recorded in the early stages of the UV-irradiations (Figure 6a). A band at nearly the same position has been previously detected in the photochemical studies performed for matrix-isolated phenol (1789 cm^{-1}) [48] and carvacrol (1775 cm^{-1}) [15] and has been ascribed to the stretching vibration of a C=O bond of a Dewar valence isomer. Therefore, an analogous species, labeled as **4** in Scheme 2, must be also formed during the UV-irradiations of **1**. It is most likely produced with the intermediacy of **3a** or **3b**, by analogy with the identical process observed for the electronically equivalent α-pyrone [52,58,59] and methyl-substituted α-pyrones [51,60]. The wavenumbers predicted for the possible structures adopted by **4** (see Table S7) fall between 1801 and 1794 cm^{-1} (A^{th} = 281–340 km mol^{-1}), see Figure 6b.

Increasing the time of exposition of the sample to the UV-radiation led to the occurrence of photodecomposition reactions, as revealed by the appearance of a narrow band at ~2137 cm^{-1} which is a spectral indication of the formation of carbon monoxide (CO) (Figure 6a and Figure S5). This band was found to continuously grow up as the time of irradiation increases, whereas the opposite behavior was observed for the bands assigned to cyclohexadienones **3** (and the open-chain ketenes **5**), see Figure S5. By analogy with our recent discussion on the photochemical behavior of matrix-isolated carvacrol [15], the most probable species resulting from the photodecomposition of thymol and its photoproducts are alkyl-substituted cyclopentadienes. These photoproducts are most likely formed by decarbonylation of the alkyl-substituted cyclohexadienones **3**, which exist in photoequilibrium with the open-chain ketenes **5** (see Scheme 2) and as long as isomers **3** are consumed, isomers **5** are also consumed (indirectly) [15], see Figure S5. These species are constituted exclusively by carbon and hydrogen atoms, thus having intrinsically low intensities in the IR spectra. Furthermore, such decarbonylated products share common groups (methyl, isopropyl) with their precursors and their new bands may overlap with already existing bands of the precursors. Therefore, it is difficult to experimentally confirm their presence in the UV-irradiated matrix.

4. Concluding Discussion

In this work, we investigated the conformational structure of monomeric thymol by a combined experimental and computational approach. Geometry optimizations at the B3LYP/6-311++G(d,p) and MP2/aug-cc-pVDZ levels of theory predicted that thymol may adopt four unique conformations defined by the mutual orientation of the vicinal isopropyl and hydroxyl groups. Two of these conformations, with the gauche-isopropyl group, are doubly degenerate and represent mirror-equivalent structures with broad and shallow double-minima on the potential energy surface of the isopropyl torsion. The two conformations with the trans-isopropyl group represent narrow and deep single minima. The two cis-OH-conformers are destabilized due to the internal repulsions between the hydrogen atoms of the hydroxyl and isopropyl groups. The two trans-OH-forms (**gt** and **tt**) are the most stable and are expected to be the most populated forms in the gas phase of thymol and (consequently) also for thymol isolated in the cryogenic matrix.

Infrared spectroscopy was used to characterize the conformational composition of thymol experimentally. In agreement with the computations, the infrared spectrum of the as-prepared matrix revealed that only the two most stable thymol conformers (trans-OH-forms **gt** and **tt**, with the OH group pointing away from the vicinal isopropyl group) co-exist in the matrix. The experimental integrated intensities of the marker bands due to the **gt** and **tt** forms, reduced by their respective computed absolute infrared intensities, suggest an approximate 3:1 ratio in favor of **gt**. The two higher energy cis-OH forms, which may have residual populations in the gas phase prior to deposition, were shown to convert into their more stable trans-OH-counterparts by fast quantum mechanical tunneling during deposition of the matrix.

By analogy with the previously studied carvacrol (differing from thymol only by position of the OH group), we attempted to promote a partial conformational isomerization between the **gt** and **tt** conformers. For this purpose, we irradiated the matrix-isolated thymol either with broadband IR light (provided by electrically heated kanthal wire) or with narrowband near-IR light (provided by an optical parametric oscillator tuned to the frequency of the first overtone of the OH-stretching mode). Despite all of these attempts, the initial populations of the **gt** and **tt** conformers did not change. The annealing of thymol isolated in a xenon matrix up to the temperatures over 75 K (i.e., up to the limit of the thermal stability of solid xenon), aiming at relaxation of the higher-energy **tt** form into the global energy minimum **gt** form, did not result in the conformational interconversion either. From these experiments, one could safely postulate that conformational populations of the **gt** and **tt** forms in a freshly deposited matrix, in the 3:1 ratio, correspond to the ratio of conformational populations of these forms in the gas phase (at room temperature) during the deposition of the sample. Taking into consideration the computed relative Gibbs free energies of the **gt** and **tt** forms at room temperature, such a conformational composition is only possible when the **gt** and **gc** forms contribute to the Boltzmann equilibrium with the weighting factors of two and the **tt** and **tc** forms with the weighting factors of one. This represents an experimental proof of the fact that the two mirror-equivalent $\mathbf{g^{+}t}$ and $\mathbf{g^{-}t}$ forms of thymol, separated by a torsional energy barrier not exceeding 0.7 kJ mol^{-1}, are indeed two individual minima, and not a single symmetry-averaged **ct** minimum.

The lack of conformational relaxation of matrix-isolated thymol was explained with the aid of computations of potential energy surfaces for the torsion of the hydroxyl and isopropyl groups in thymol and in the related molecules. Furthermore, the torsional barrier for isopropyl group in thymol is nearly 2.5 times higher than in its isomeric carvacrol. On the other hand, the torsional barrier for the hydroxyl group in carvacrol and thymol are approximately equal, but in thymol it is about a half as low compared to the torsional barrier of its isopropyl group. In our mechanistic interpretation, the energy provided by vibrational excitation (infrared or near-IR) of thymol is dissipated much more efficiently via the hydroxyl torsion, and therefore the isopropyl torsion does not occur.

The matrix-isolated thymol was subsequently irradiated with broadband UV-light ($\lambda > 200$ nm), and the resulting transformations were monitored by IR spectroscopy. As is typical of phenol derivatives, the photoexcitation of thymol resulted in production of corresponding alkyl-substituted cyclohexadienones. Mechanistically, such a photochemical behavior was explained in terms of the OH group cleavage (with generation of an alkyl-substituted phenoxyl radical), followed by recombination of the released H-atom (also a radical) at the *ortho*- or *para*- positions of the ring (with respect to the CO group). The natural spin densities of the phenoxyl-type radical, extracted from the NBO calculations, indicate that precisely the *ortho*- or *para*- carbon atoms of the ring are the most favorable positions for the above-mentioned recombination of the radical pair. The cyclohexadienone photoproducts were found to undergo further isomerizations, yielding Dewar isomeric species and open-chain conjugated ketenes. Decarbonylation of the photoproducts was also observed for longer irradiation times.

On the whole, the present investigation fills a gap in the knowledge about the structural, vibrational, and photochemical properties of monomeric thymol. This fundamental knowledge constitutes a basis for the understanding of the bioactivity of this and related compounds.

Supplementary Materials: The following supporting information can be downloaded at: https://www.mdpi.com/article/10.3390/photochem2020028/s1. Tables S1 and S2, Cartesian coordinates for the conformers of thymol optimized at B3LYP/6-311++G(d,p) and MP2/aug-cc-pVDZ levels of theory; Table S3, Scaled wavenumbers (cm^{-1}) and IR intensities (km mol^{-1}) calculated for the thymol conformers by means of B3LYP harmonic vibrational calculations; Tables S4–S7, Geometries and selected energetic and vibrational parameters calculated at the B3LYP level for different photoproducts resulting from the UV-isomerizations of matrix-isolated thymol; Figure S1, B3LYP potential energy scans for the intramolecular torsion of the isopropyl group computed for thymol, carvacrol, and *p*-cymene; Figure S2, Detailed comparison of the experimental spectra of thymol isolated in Ar and Xe matrices with the spectra calculated for the four conformers of thymol; Figure S3, Fragment

(7100–7020 cm^{-1}) of the near-IR spectrum of thymol isolated in Xe showing the band assigned to the first OH-stretching overtone; Figure S4, Natural spin densities computed for the heavy atoms of the two conformers of the phenoxyl-type radical of thymol by means of a Natural Bond Orbital (NBO) analysis carried out at the UB3LYP/6-311++G(d,p) level of theory; Figure S5, Evolution of the bands due to photoproducts emerging in the 2160–2080 cm^{-1} and 1690–1650 cm^{-1} regions, as function of the time of UV-irradiation.

Author Contributions: A.J.L.J., conceptualization, investigation, computations, writing—original draft preparation; C.M.N., writing—review and editing, formal analysis, project administration; I.R., laboratory work, computations, writing—review and editing, formal analysis. All authors have read and agreed to the published version of the manuscript.

Funding: This work was supported by Project POCI-01-0145-FEDER-028973 funded by FEDER, via Portugal 2020-POCI, and by National Funds via the Portuguese Foundation for Science and Technology (FCT). The Coimbra Chemistry Centre—Institute of Molecular Sciences (CQC-IMS) is supported by FCT through projects UIDB/00313/2020 and UIDP/00313/2020 co-funded by COMPETE and the IMS special complementary funds provided by FCT. The Chemical Process Engineering and Forest Products Research Centre (CIEPQPF) is supported by FCT through projects UIDB/EQU/00102/2020 and UIDP/EQU/00102/2020 (National Funds). C.M.N. acknowledges FCT for an Auxiliary Researcher grant. The authors also acknowledge LaserLab Coimbra for experimental facilities.

Institutional Review Board Statement: Not applicable.

Informed Consent Statement: Not applicable.

Acknowledgments: The authors acknowledge Katarzyna M. Marzec and José P. L. Roque for their participation in some of the matrix-isolation experiments.

Conflicts of Interest: The authors declare no conflict of interest.

References

1. Nagoor Meeran, M.F.; Javed, H.; Al Taee, H.; Azimullah, S.; Ojha, S.K. Pharmacological properties and molecular mechanisms of thymol: Prospects for its therapeutic potential and pharmaceutical development. *Front. Pharmacol.* **2017**, *8*, 380. [CrossRef]
2. Sahoo, C.R.; Paidesetty, S.K.; Padhy, R.N. The recent development of thymol derivative as a promising pharmacological scaffold. *Drug Dev. Res.* **2021**, *82*, 1079–1095. [CrossRef]
3. Escobar, A.; Pérez, M.; Romanelli, G.; Blustein, G. Thymol bioactivity: A review focusing on practical applications. *Arab. J. Chem.* **2020**, *13*, 9243–9269. [CrossRef]
4. Jamali, T.; Kavoosi, G.; Jamali, Y.; Mortezazadeh, S.; Ardestani, S.K. In-vitro, in-vivo, and in-silico assessment of radical scavenging and cytotoxic activities of *Oliveria decumbens* essential oil and its main components. *Sci. Rep.* **2021**, *11*, 14281. [CrossRef]
5. Bautista-Hernández, I.; Aguilar, C.N.; Martínez-Ávila, G.C.G.; Torres-León, C.; Ilina, A.; Flores-Gallegos, A.C.; Kumar Verma, D.; Chávez-González, M.L. Mexican oregano (Lippia graveolens Kunth) as source of bioactive compounds: A review. *Molecules* **2021**, *26*, 5156. [CrossRef]
6. Nieto, G. A review on applications and uses of thymus in the food industry. *Plants* **2020**, *9*, 961. [CrossRef]
7. Pandey, S.K.; Upadhyay, S.; Tripathi, A.K. Insecticidal and repellent activities of thymol from the essential oil of *Trachyspermum ammi* (Linn) Sprague seeds against Anopheles stephensi. *Parasitol. Res.* **2009**, *105*, 507–512. [CrossRef]
8. Scoralik, M.G.; Daemon, E.; de Oliveira Monteiro, C.M.; Maturano, R. Enhancing the acaricide effect of thymol on larvae of the cattle tick Rhipicephalus microplus (Acari: Ixodidae) by solubilization in ethanol. *Parasitol. Res.* **2012**, *110*, 645–648. [CrossRef] [PubMed]
9. Thozet, A.; Perrin, M. Structure of 2-isopropyl-5-methylphenol (thymol). *Acta Crystallogr. Sect. B* **1980**, *36*, 1444–1447. [CrossRef]
10. Schmitz, D.; Shubert, V.A.; Giuliano, B.M.; Schnell, M. The broadband microwave spectra of the monoterpenoids thymol and carvacrol: Conformational landscape and internal dynamics. *J. Chem. Phys.* **2014**, *141*, 034304. [CrossRef]
11. Sin, K.-R.; Kim, C.-J.; Ko, S.-G.; Hwang, T.-M.; Han, Y.-N.; Pak, Y.-N. Inclusion of thymol into cucurbiturils: Density functional theory approach with dispersion correction and natural bond orbital analysis. *J. Inclusion Phenom. Macrocycl. Chem.* **2022**, *102*, 533–542. [CrossRef]
12. Saraiva, A.G.Q.; Saraiva, G.D.; Albuquerque, R.L.; Nogueira, C.E.S.; Teixeira, A.M.R.; Lima, L.B.; Cruz, B.G.; de Sousa, F.F. Chemical analysis and vibrational spectroscopy study of essential oils from Lippia sidoides and of its major constituent. *Vib. Spectrosc.* **2020**, *110*, 103111. [CrossRef]
13. Rajkumar, P.; Selvaraj, S.; Suganya, R.; Velmurugan, D.; Gunasekaran, S.; Kumaresan, S. Vibrational and electronic spectral analysis of thymol an isomer of carvacrol isolated from Trachyspermum ammi seed: A combined experimental and theoretical study. *Chem. Data Collect.* **2018**, *15–16*, 10–31. [CrossRef]

14. Beć, K.B.; Grabska, J.; Kirchler, C.G.; Huck, C.W. NIR spectra simulation of thymol for better understanding of the spectra forming factors, phase and concentration effects and PLS regression features. *J. Mol. Liq.* **2018**, *268*, 895–902. [CrossRef]
15. Lopes Jesus, A.J.; Fausto, R.; Reva, I. Conformational Space, IR-Induced, and UV-induced chemistry of carvacrol isolated in a low-temperature argon matrix. *J. Phys. Chem. A* **2021**, *125*, 8215–8229. [CrossRef] [PubMed]
16. Becke, A.D. Density-functional exchange-energy approximation with correct asymptotic behavior. *Phys. Rev. A* **1988**, *38*, 3098–3100. [CrossRef]
17. Lee, C.T.; Yang, W.T.; Parr, R.G. Development of the Colle-Salvetti correlation-energy formula into a functional of the electron-density. *Phys. Rev. B* **1988**, *37*, 785–789. [CrossRef] [PubMed]
18. Vosko, S.H.; Wilk, L.; Nusair, M. Accurate spin-dependent electron liquid correlation energies for local spin density calculations: A critical analysis. *Can. J. Phys.* **1980**, *58*, 1200–1211. [CrossRef]
19. Møller, C.; Plesset, M.S. Note on an approximation treatment for many-electron systems. *Phys. Rev.* **1934**, *46*, 618–622. [CrossRef]
20. Pople, J.A.; Head-Gordon, M.; Raghavachari, K. Quadratic configuration interaction. A general technique for determining electron correlation energies. *J. Chem. Phys.* **1987**, *87*, 5968–5975. [CrossRef]
21. Reva, I.; Lopes Jesus, A.J.; Nunes, C.M.; Roque, J.P.L.; Fausto, R. UV-Induced Photochemistry of 1,3-Benzoxazole, 2-Isocyanophenol, and 2-Cyanophenol Isolated in Low-Temperature Ar Matrixes. *J. Org. Chem.* **2021**, *86*, 6126–6137. [CrossRef] [PubMed]
22. Zhurko, G.A. Chemcraft—Graphical Program for Visualization of Quantum Chemistry Computations, Version 1.8. 2020. Available online: http://www.chemcraftprog.com (accessed on 18 May 2022).
23. Frisch, M.J.; Trucks, G.W.; Schlegel, H.B.; Scuseria, G.E.; Robb, M.A.; Cheeseman, J.R.; Scalmani, G.; Barone, V.; Mennucci, B.; Petersson, G.A.; et al. *GAUSSIAN 09, Revision D.01*; Gaussian, Inc.: Wallingford, CT, USA, 2013.
24. Teixeira, F.; Cordeiro, M.N.D.S. Improving vibrational mode interpretation using bayesian regression. *J. Chem. Theory Comput.* **2019**, *15*, 456–470. [CrossRef] [PubMed]
25. Lesarri, A.; Shipman, S.T.; Neill, J.L.; Brown, G.G.; Suenram, R.D.; Kang, L.; Caminati, W.; Pate, B.H. Interplay of phenol and isopropyl isomerism in propofol from broadband chirped-pulse microwave spectroscopy. *J. Am. Chem. Soc.* **2010**, *132*, 13417–13424. [CrossRef]
26. Zhao, Y.; Jin, Y.; Hao, J.; Yang, Y.; Wang, L.; Li, C.; Jia, S. Rotamers of p-isopropylphenol studied by hole-burning resonantly enhanced multiphoton ionization and mass analyzed threshold ionization spectroscopy. *Spectrochim. Acta Part A* **2019**, *207*, 328–336. [CrossRef] [PubMed]
27. Richardson, P.R.; Chapman, M.A.; Wilson, D.C.; Bates, S.P.; Jones, A.C. The nature of conformational preference in a number of p-alkyl phenols and p-alkyl benzenes. *Phys. Chem. Chem. Phys.* **2002**, *4*, 4910–4915. [CrossRef]
28. Schaefer, T.; Addison, B.M.; Sebastian, R.; Wildman, T.A. Orientations of the hydroxyl and isopropyl groups in the cis and trans conformers of 2-isopropylphenol and 2-isopropyl-6-methylphenol. *Can. J. Chem.* **1981**, *59*, 1656–1659. [CrossRef]
29. Rozenberg, M.; Fausto, R.; Reva, I. Variable temperature FTIR spectra of polycrystalline purine nucleobases and estimating strengths of individual hydrogen bonds. *Spectrochim. Acta Part A* **2021**, *251*, 119323. [CrossRef] [PubMed]
30. Lopes Jesus, A.J.; Rosado, M.T.S.; Leitão, M.L.P.; Redinha, J.S. Molecular structure of butanediol isomers in gas and liquid states: Combination of DFT calculations and infrared spectroscopy studies. *J. Phys. Chem. A* **2003**, *107*, 3891–3897. [CrossRef]
31. Lopes Jesus, A.J.; Rosado, M.T.S.; Reva, I.; Fausto, R.; Eusébio, M.E.S.; Redinha, J.S. Structure of isolated 1,4-Butanediol: Combination of MP2 calculations, NBO analysis, and matrix-isolation infrared spectroscopy. *J. Phys. Chem. A* **2008**, *112*, 4669–4678. [CrossRef]
32. Lopes Jesus, A.J.; Rosado, M.T.S.; Reva, I.; Fausto, R.; Eusébio, M.E.; Redinha, J.S. Conformational study of monomeric 2,3-Butanediols by matrix-isolation infrared spectroscopy and DFT calculations. *J. Phys. Chem. A* **2006**, *110*, 4169–4179. [CrossRef] [PubMed]
33. Rosado, M.T.S.; Lopes Jesus, A.J.; Reva, I.D.; Fausto, R.; Redinha, J.S. Conformational cooling dynamics in matrix-isolated 1,3-Butanediol. *J. Phys. Chem. A* **2009**, *113*, 7499–7507. [CrossRef]
34. Lopes Jesus, A.J.; Nunes, C.M.; Reva, I.; Pinto, S.M.V.; Fausto, R. Effects of entangled IR radiation and tunneling on the conformational interconversion of 2-Cyanophenol. *J. Phys. Chem. A* **2019**, *123*, 4396–4405. [CrossRef]
35. Lopes Jesus, A.J.; Reva, I.; Nunes, C.M.; Roque, J.P.L.; Pinto, S.M.V.; Fausto, R. Kinetically unstable 2-isocyanophenol isolated in cryogenic matrices: Vibrational excitation, conformational changes and spontaneous tunneling. *Chem. Phys. Lett.* **2020**, *742*, 137069. [CrossRef]
36. Akai, N.; Kudoh, S.; Takayanagi, M.; Nakata, M. Cis-Trans isomerization equilibrium in hydroquinone in low-temperature argon and xenon matrices studied by FTIR spectroscopy. *Chem. Phys. Lett.* **2002**, *356*, 133–139. [CrossRef]
37. Akai, N.; Kudoh, S.; Nakata, M. Photoisomerization and tunneling isomerization of tetrachlorohydroquinone in a low-temperature argon matrix. *J. Phys. Chem. A* **2003**, *107*, 3655–3659. [CrossRef]
38. Borden, W.T. Reactions that involve tunneling by carbon and the role that calculations have played in their study. *WIREs Comput. Mol. Sci.* **2016**, *6*, 20–46. [CrossRef]
39. Nunes, C.M.; Reva, I.; Fausto, R. Direct observation of tunnelling reactions by matrix isolation spectroscopy. In *Tunnelling in Molecules: Nuclear Quantum Effects from Bio to Physical Chemistry*; Kästner, J., Kozuch, S., Eds.; The Royal Society of Chemistry: Cambridge, UK, 2021; pp. 1–60. [CrossRef]
40. Pettersson, M.; Lundell, J.; Khriachtchev, L.; Räsänen, M. IR spectrum of the other rotamer of formic acid, cis-HCOOH. *J. Am. Chem. Soc.* **1997**, *119*, 11715–11716. [CrossRef]

41. Maçôas, E.M.S.; Khriachtchev, L.; Pettersson, M.; Fausto, R.; Räsänen, M. Rotational isomerism in acetic acid: The first experimental observation of the high-energy conformer. *J. Am. Chem. Soc.* **2003**, *125*, 16188–16189. [CrossRef]
42. Lapinski, L.; Reva, I.; Rostkowska, H.; Halasa, A.; Fausto, R.; Nowak, M.J. Conformational Transformation in Squaric Acid Induced by Near-IR Laser Light. *J. Phys. Chem. A* **2013**, *117*, 5251–5259. [CrossRef]
43. Kuş, N.; Fausto, R. Effects of the matrix and intramolecular interactions on the stability of the higher-energy conformers of 2-fluorobenzoic acid. *J. Chem. Phys.* **2017**, *146*, 124305. [CrossRef]
44. Gerbig, D.; Schreiner, P.R. Hydrogen-Tunneling in Biologically Relevant Small Molecules: The Rotamerizations of α-Ketocarboxylic Acids. *J. Phys. Chem. B* **2015**, *119*, 693–703. [CrossRef]
45. Bazsó, G.; Magyarfalvi, G.; Tarczay, G. Tunneling lifetime of the ttc/VIp conformer of glycine in low-temperature matrices. *J. Phys. Chem. A* **2012**, *116*, 10539–10547. [CrossRef] [PubMed]
46. Lopes Jesus, A.J.; Reva, I.; Araujo-Andrade, C.; Fausto, R. Conformational changes in matrix-isolated 6-methoxyindole: Effects of the thermal and infrared light excitations. *J. Chem. Phys.* **2016**, *144*, 124306. [CrossRef]
47. Marzec, K.M.; Reva, I.; Fausto, R.; Proniewicz, L.M. Comparative matrix isolation infrared spectroscopy study of 1,3- and 1,4-diene monoterpenes (α-Phellandrene and γ-Terpinene). *J. Phys. Chem. A* **2011**, *115*, 4342–4353. [CrossRef] [PubMed]
48. Giuliano, B.M.; Reva, I.; Lapinski, L.; Fausto, R. Infrared spectra and ultraviolet-tunable laser induced photochemistry of matrix-isolated phenol and phenol-d_5. *J. Chem. Phys.* **2012**, *136*, 024505. [CrossRef]
49. Giuliano, B.M.; Melandri, S.; Reva, I.; Fausto, R. Conformational space and photochemistry of tyramine isolated in argon and xenon cryomatrixes. *J. Phys. Chem. A* **2013**, *117*, 10248–10259. [CrossRef]
50. Barnes, A.J. Matrix isolation vibrational spectroscopy as a tool for studying conformational isomerism. *J. Mol. Struct.* **1984**, *113*, 161–174. [CrossRef]
51. Breda, S.; Lapinski, L.; Reva, I.; Fausto, R. 4,6-Dimethyl-α-pyrone: A matrix isolation study of the photochemical generation of conjugated ketene, Dewar valence isomer and 1,3-dimethyl-cyclobutadiene. *J. Photochem. Photobiol. A* **2004**, *162*, 139–151. [CrossRef]
52. Breda, S.; Reva, I.; Lapinski, L.; Fausto, R. Matrix isolation FTIR and theoretical study of α-pyrone photochemistry. *Phys. Chem. Chem. Phys.* **2004**, *6*, 929–937. [CrossRef]
53. Tidwell, T.T. Spectroscopy and physical properties of ketenes. In *Ketenes II*; John Wiley and Sons: Hoboken, NJ, USA, 2006; pp. 27–53.
54. Kuş, N.; Sagdinc, S.; Fausto, R. Infrared spectrum and UV-induced photochemistry of matrix-isolated 5-Hydroxyquinoline. *J. Phys. Chem. A* **2015**, *119*, 6296–6308. [CrossRef] [PubMed]
55. Krupa, J.; Olbert-Majkut, A.; Reva, I.; Fausto, R.; Wierzejewska, M. Ultraviolet-tunable laser induced phototransformations of matrix isolated isoeugenol and eugenol. *J. Phys. Chem. B* **2012**, *116*, 11148–11158. [CrossRef]
56. Samanta, A.K.; Pandey, P.; Bandyopadhyay, B.; Chakraborty, T. Keto–enol tautomers of 1,2-cyclohexanedione in solid, liquid, vapour and a cold inert gas matrix: Infrared spectroscopy and quantum chemistry calculation. *J. Mol. Struct.* **2010**, *963*, 234–239. [CrossRef]
57. Miyazaki, J.; Toh, S.Y.; Moore, B.; Djuricanin, P.; Momose, T. UV photochemistry of 1,3-cyclohexadiene isolated in solid parahydrogen. *J. Mol. Struct.* **2021**, *1224*, 128986. [CrossRef]
58. Chapman, O.L.; McIntosh, C.L.; Pacansky, J. Photochemistry of a-Pyrone in Argon at 8 °K. *J. Am. Chem. Soc.* **1973**, *95*, 244–246. [CrossRef]
59. Pong, R.G.S.; Shirk, J.S. Photochemistry of α-Pyrone in solid argon. *J. Am. Chem. Soc.* **1973**, *95*, 248–249. [CrossRef]
60. Breda, S.; Lapinski, L.; Fausto, R.; Nowak, M.J. Photoisomerization reactions of 4-methoxy- and 4-hydroxy-6-methyl-α-pyrones: An experimental matrix isolation and theoretical density functional theory study. *Phys. Chem. Chem. Phys.* **2003**, *5*, 4527–4532. [CrossRef]